

GroundGazer: Camera-based indoor localization of mobile robots with millimeter accuracy at low cost

Sven Hinderer, Jakob Hüsken, Bohan Sun, Bin Yang

Abstract—Highly accurate indoor localization systems with mm positioning accuracy are currently very expensive. They include laser trackers, total stations, and motion capture systems relying on multiple high-end cameras. In this work, we introduce a high-accuracy, planar indoor localization system named GroundGazer (GG) for autonomous mobile robots (AMRs). GG estimates the AMR’s position with mm and its heading with sub-degree accuracy. The system requires only a monocular (fisheye) camera, a chessboard floor, and an optional laser diode. Our system is simple and low-cost, easy to set up, portable, robust, scalable to large areas and robot swarms, and extendable to 3D position and orientation estimation.

Keywords—Indoor localization, mobile robots, computer vision

I. INTRODUCTION

Benchmarking lower-accuracy indoor positioning systems with up to cm localization accuracy requires localization approaches with reliable mm positioning accuracy. Currently, such systems are very costly (generally > 1000 \$, with costs rising quickly with increasing size of the coverage area). In this work, we introduce a novel camera-based indoor localization system for AMRs which achieves mm localization and sub-degree heading accuracy at multitudes lower cost than existing systems of similar precision. We name it GroundGazer, as the camera placed on the AMR gazes at the passive position references on the ground.

Before describing the GG system, we give an introduction into currently existing and researched indoor localization technologies for AMRs with mm positioning accuracy. For an overview of general indoor localization technologies, we refer to the surveys in [1] and [2]. Comprehensive overviews of optical indoor localization systems can be found in [3] and [4].

A. Localization technologies with mm positioning accuracy

Motion capture systems consist of passive infrared (IR) markers placed on the to be tracked AMR. With one marker, 3D positioning is possible. A minimum of three non-collinear markers enable 3D position and orientation estimation. Motion capture systems like the commercial systems by Qualisys and Vicon¹ are very popular in robotics and industry. While capable of sub-mm 3D localization and sub-degree orientation estimation, they require line of sight (LOS), multiple high-end IR cameras, and become very expensive if large areas are to be observed. Further, the IR cameras not installed around the AMR complicate the time synchronization when the motion

capture system is used as reference for another localization system with sensors installed on the AMR. Highly accurate time synchronization is required, since otherwise the mm accuracy is lost through badly matched time stamps.

Total stations (tachymeters) pose a another solution for 3D position estimation with mm or sub-mm accuracy, e.g. used as 3D position reference system in [5]. Total stations enable long range sensing, but like motion capture systems, they are expensive and require LOS and more complex time synchronization mechanisms.

A novel sub-mm positioning system with long distance capabilities based on radio signals and interferometry that has recently seen real-world deployments is developed by Koherent².

Radio frequency (RF)-based backscatter systems using frequency modulated continuous wave (FMCW) radar and (semi-)active reflective tags (e.g. Van-Atta arrays) that modulate the reflected radar signal can also achieve 3D mm localization accuracy using high-precision range estimates of the tags and multilateration (MLAT) [6] or triangulation [7] for positioning. The system in [6] could also demonstrate good performance with large radar-tag distance.

In acoustic ultrasound systems, small timing errors in the measured time of flight (ToF) of the signals or in the synchronization between anchors cause lower positioning errors than in RF-based ultra wideband (UWB) systems. The reason lies in the much lower propagation speed of acoustic waves. The company ZeroKey claims real-time and up to 1.5 mm 3D positioning accuracy with their commercial Quantum RLTS 2.0 system, given 6 acoustic anchors with ideal geometric placement [8]. Positioning is performed with multiple active acoustic anchors and ToF measurements between anchors and the to be tracked AMR and by applying MLAT for localization.

While ToF-based localization with UWB systems only gives dm to cm accuracy, recent studies show mm accuracy by combining initial, coarse ToF-based range estimates with refined, ambiguity-resolved phased-based range estimates [9].

Deep learning-based channel state information (CSI) fingerprinting with a massive multiple input multiple output (MIMO) system could recently achieve mm accuracy in a small area and under LOS conditions [10]. However, the performance of such system degrades with changes in the environment, causing domain shifts between the measured fingerprints during inference and the pre-recorded fingerprint database.

All authors are with the Institute of Signal Processing and System Theory, University of Stuttgart, Stuttgart, Germany. `firstname.lastname@iss.uni-stuttgart.de`

¹Available at: <https://www.qualisys.com/> and <https://www.vicon.com/>.

²Available at: <https://koherent.io/>

Fiducial markers pose another solution for highly precise localization. In [11], the combination of high-end binocular cameras and custom markers achieves sub-mm localization accuracy. Downsides are again the high cost of the cameras and the required LOS. The authors of [12] proposed a docking system with sub-mm 2D positioning accuracy using quick response (QR) codes and an RGB camera. Although low-cost, the very small camera-QR code distance and the need for many QR codes limit its use for general AMR localization.

Other systems with (sub-)mm accuracy based on visual markers, laser projections, magnetic fields, laser trackers, pseudolites, and infrared laser beams (iGPS) can be found in [3] and [13].

B. Contributions

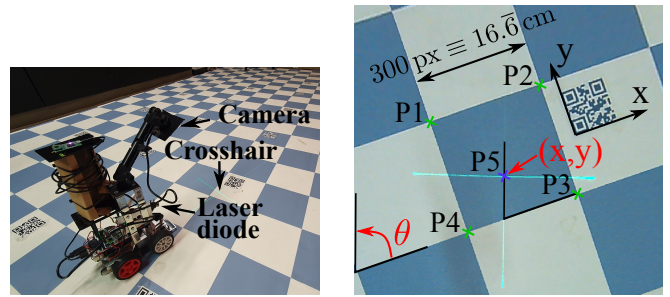
We introduce a novel mm accuracy localization approach with the intended application to serve as reference for less accurate indoor positioning systems. The GG prototype described in this paper requires only a chessboard floor (or similar grid pattern), a camera (here a global shutter RGB fisheye camera), and an optional laser diode, i.e. low-cost off-the-shelf components. Currently, it only allows for planar position (x, y) and heading θ estimation, which is sufficient for our application as reference system for planar AMR position and heading estimation with known or irrelevant height, roll and pitch. In Sec. VI, we discuss an adaption that yields 3D position and orientation estimates, but has higher computational complexity and possibly lower accuracy.

The idea for our GG system originates from [14]. They developed a fiducial marker localization system that requires a chessboard floor in addition to the fiducial markers, where a car is equipped with multiple fiducial markers placed on a plate mounted at the front of the car. To evaluate the positioning accuracy of this system, they installed two point laser diodes that project two points from the front and the back of the car onto the chessboard floor beneath it. The corner coordinates of the chessboard serve as position references and they measure the two laser point locations on the floor as ground truth by hand. The laser point at the front of the car is used as vehicle reference position and the heading is derived from the orientation of the line connecting both points w.r.t. to the chessboard. Our GG system builds on that idea, resulting in a highly accurate, camera-based indoor localization system.

C. System overview

Our localization system is depicted in Fig. 1a. It consists of an AMR, which is equipped with an RGB fisheye camera (< 100 \$) with large field-of-view (FoV) and global shutter. Global shutter cameras have lower motion blur than rolling shutter cameras due to parallel collection of all pixels. The camera is facing the ground and a green laser diode (negligible cost) projects a crosshair on said ground. The ground itself is made up of a chessboard pattern with well known grid size.

The localization system works by detecting the crosshair in a square of the chessboard. We specifically selected a blue and white chessboard floor and a green laser diode, as



(a) Our system in the laboratory equipped with a chessboard floor and QR codes. The AMR has a ground facing camera and a laser diode that projects a crosshair on the floor at the front.

(b) 2D position and heading estimation using the detected crosshair (P5), the chessboard square corners (P1-P4), and the x -direction chessboard lines. The globally known square corner coordinates through the QR codes enable accurate, global positioning.

Fig. 1: Overview of our GG localization system in a) and conceptual depiction of the localization method in b).

green lasers are most easily visible and other commercially available black and white chessboard floors complicate the crosshair detection, caused by the large difference in laser reflective behavior between black and white squares. The camera image is calibrated such that the heading of the AMR can be estimated based on the orientation of the chessboard in the image. The corner coordinates of the chessboard squares are known and serve as passive position references for AMR localization.

Since the chessboard corner coordinates are ambiguous to the camera which only observes a small, local area of the periodic chessboard pattern, we additionally equip the floor with different QR codes as global position and orientation references. All QR codes are oriented in the same direction, parallel to the chessboard lines, and their corners can therefore be used to extract the x - and y -directions of the chessboard lines in global coordinates. The QR code IDs allow for identification of the QR code squares and global positioning. By measuring the distance in x - and y -direction between a detected QR code square center and the center of the square in which the crosshair lies (neglecting the trivial case where they are identical), we can further identify the crosshair square and its known corner coordinates without requiring a QR code in each square. Measuring the relative position of the crosshair w.r.t. its square corners (at least three corners are required to build a coordinate system, but we use four corners as known from a detected square) gives the AMR's position and the angle between the chessboard lines in x -direction and the vertical image direction gives its heading. The AMR position is assumed as the crosshair position. An image describing the AMR positioning is shown in Fig. 1b.

High position and heading accuracy is enabled by placing the camera close to the ground and by precise estimation of the chessboard square corners, the chessboard lines, and the crosshair center. For this prototype, a camera with fisheye lens

was chosen because of their large FoV, allowing observation of multiple chessboard squares with a small camera-ground distance. The whole processing chain, which transforms the initial fisheye image, detects the QR codes, the crosshair, and the chessboard square corners, and finally estimates the AMR’s position and heading, is described in Sec. III.

II. RELATED WORKS WITH GROUND GAZING CAMERAS

In this section, we focus on closely related systems that employ ground gazing cameras for global localization. A general overview of indoor positioning systems with (sub)-mm accuracy for AMRs was given in Sec. I-A.

One approach to global localization using ground gazing cameras is by avoiding external infrastructure, i.e. localization using only the given ground texture. Relative positioning can be realized through simultaneous localization and mapping (SLAM) [15], but we are interested in absolute, global positioning. Such positioning is possible with feature-matching of images collected during inference with a pre-collected image database of the ground [16]–[20]. The advantage of this is the applicability in (ideally) any kind of environment without requiring new infrastructure, making it a practical method e.g. for warehousing. However, feature-matching requires an expensive measurement campaign for collection of reference images of the floor with accurate ground truth, e.g. from motion capture systems. These approaches have also shown varying reliability for different surfaces [17] and the position errors are in the low cm range (ignoring outliers, but also not yet using temporal correlations) and the heading errors are in the low degree range [20]. Positioning errors further seem to increase with coverage area (map size) [20]. The commercial feature-matching-based systems by Accerion are reported to deliver sub-mm accuracy, but only for repeated tasks such as docking, where the task was accurately executed before, while stating cm accuracy for global localization³. For relative localization, features of successive images can similarly be matched to build a vision-based odometer [21]. While feature-matching approaches require no additional infrastructure, we argue that using known position references is the more suitable approach for reference systems due to higher accuracy, robustness, easier setup, and lower hardware requirements.

Various approaches have considered placing infrastructure on the floor for absolute, global localization. In [22], ArUco markers are distributed on the floor and combined with odometry in an Extended Kalman filter (EKF) for AMR localization. However, they don’t give localization accuracy results. AMR localization with a simulated grid of Apriltags yields cm accuracy in [23]. QR codes are also commonly applied, e.g. for a heeled robotic walking assistant in [24], achieving dm accuracy with additional odometry and gyroscope data. In [25], a drone with a ground facing camera is localized with a QR code grid on the floor and using the nearest QR code for position and heading estimation, showing cm accuracy.

³Due to the limited product specifications on the company website (no published data sheets), we are relying on the information given on their Youtube channel found at <https://www.youtube.com/@accerion4564>.

Different fiducial marker types are benchmarked regarding their detection behavior in ground-based localization in [26].

It should be noted, however, that we believe low-cost mm accuracy with floor installations of ArUco, AprilTag, QR codes, or similar fiducial markers is possible. With ceiling installations of ArUco markers and much larger camera-marker distances, we could achieve low cm accuracy in previous work [27] and [12] reports sub-mm accuracy with very small camera-QR code distance. Similar commercial systems can also be found. One example is the company Hikrobot, which provides AMRs and vision-based localization solutions using a visual marker grid on the floor for warehousing, logistics etc.⁴ The Hercules AMR by Amazon robotics is another commercial system using such floor marker grid for navigation.

Opposed to existing systems, we can deliver absolute 2D position and heading estimates with mm and sub-degree accuracy at low cost and with minimal setup. Our processing can likely also be sped-up through further optimization as discussed in Sec. VI to enable near real-time mm accuracy during online processing with common AMR velocities of $>1 \frac{\text{m}}{\text{s}}$, factoring in additional delays from exposure time and image transmission to the processor (10 ms delay at $1 \frac{\text{m}}{\text{s}}$ causes 10 mm error, i.e. cm online accuracy). This online bottleneck might be solved by integrating a high-frequency inertial measurement unit (IMU). Neither current SLAM nor feature-matching approaches can produce this due to higher processing times. To the best of our knowledge, no system like GG exists right now for indoor localization of AMRs that offers a similar combination of high accuracy, low cost, simplicity, easy setup, scalability, portability, and fast processing.

III. GROUNDGAZER

A. Image transformation

The first step of our processing is the transformation of the distorted and skewed image collected by the fisheye camera to a top-down view of the chessboard floor. This step consists of two transformations. First, the fisheye image needs to be undistorted. We apply the built-in `undistort` function from OpenCV [28]⁵. This function takes as input the distorted fisheye image, the intrinsic matrix \mathbf{K} of the camera, and its distortion coefficient vector \underline{d} , and outputs the undistorted image. The intrinsic matrix \mathbf{K} and the distortion coefficient vector \underline{d} have to be determined beforehand by camera calibration. We used a printed chessboard pattern and the `calibrateCamera` function for this task. A distorted fisheye image and the result after undistortion are shown in Fig. 2a and Fig. 2b, respectively. The second step transforms the undistorted image to a top-down view. This can be realized with the `warpPerspective` function, which takes the undistorted image and the homography matrix as input and gives the top-down view. The homography relates the

⁴Available at: <https://www.hikrobotics.com/en/>.

⁵If not specified otherwise, we always refer to OpenCV functions for the remainder of the paper.

undistorted and the top-down view. It can be estimated offline with the `findHomography` function and corresponding image points of the two views. We define a square of size (300, 300) pixels with horizontal and vertical edges for the wanted top-down view after perspective transformation and we select the four corresponding chessboard corner points from the undistorted image. The perspective transformed top-down image is given in Fig. 2c. The AMR orientation has to match the direction of the calibration square, i.e. in our case $\theta = 90^\circ$, to align the heading with the transformed chessboard orientation used for heading estimation. Alternatively, one could use the angle between a similarly calibrated, vertical crosshair line that points in heading direction and the x -direction chessboard line. This option would make heading estimation independent of the camera orientation and thus of camera vibrations. However, it is still susceptible to lesser laser diode vibrations and it makes heading estimation dependent on the crosshair line detection, which is worse than the chessboard line detection due to broader edges, crosshair distortion on uneven ground etc., and therefore not chosen.

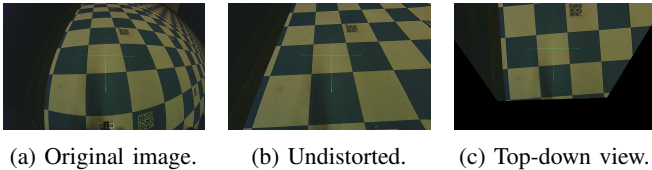


Fig. 2: Transformation of an original image recorded with an AMR heading slightly below 90° in a) through undistortion in b) and perspective transformation in c).

B. QR code detection and masking

QR codes are detected using OpenCV, which outputs the four corner points of the QR code in known order. This gives the global orientation information, previously shown in Fig. 1b. The QR code ID is extracted with the `pyzbar` library⁶, as it gave better results than OpenCV. The QR ID enables identification of the respective chessboard square. By computing the difference in x and y between the square centers where the QR code is detected and where the crosshair is detected, the QR ID also gives us the square in which the crosshair lies and thus global localization capabilities.

Since the QR codes would disturb the successive image processing operations, we mask them out. Therefore, the average color around the detected QR code is computed and the region of the QR code is replaced with a slightly larger rectangle of this color. This masking procedure might also mask out parts of the crosshair if it lies on a QR code. The QR code masking could be improved in future work, but our experiments have shown that our system can cope with irregular missed crosshair detections. By proper parametrization of the Hough transform [29] in the crosshair detection, we can also detect an incomplete crosshair.

⁶Available at: <https://pypi.org/project/pyzbar/>.

C. Crosshair detection and masking

The green crosshair can be extracted by filtering the image with a mask that keeps the green image parts. This mask has to be carefully tuned, as both the different colors of the chessboard and varying illumination condition influence the detected crosshair color. We therefore apply a concatenation of multiple masks. The first mask filters out all pixels with low green values. We then convert the image to the HSV color space, which was more robust than only working in the RGB space. Three additional masks filter out pixels with low saturation, low hue, and pixels where the sum of hue and value is low. A combined crosshair mask is found in Fig. 3a. The horizontal and vertical lines in a region of 150 pixels around the estimated crosshair position from the previous time step are then found by Hough transformation, clustered into lines with similar angle and start- and endpoints, and the start and end x -values of the clustered lines are averaged for the vertical, and the y -values for the horizontal line. The crosshair location in image coordinates is then estimated as the intersection of the horizontal and vertical crosshair lines. The final crosshair lines and the detected crosshair position are shown in Fig. 3b. To not disturb the chessboard square detection, we mask out the crosshair with an extended and broadened version of the detected crosshair.

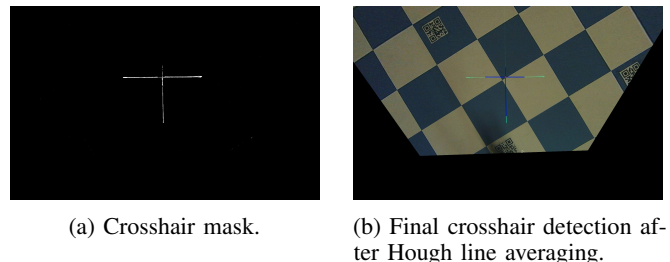


Fig. 3: Crosshair detection process.

If the crosshair is not detected or if there is a large deviation from the expected crosshair position, we use an average of the previous crosshair positions as estimate. In principle, our system can work without the laser diode by calibration one initial crosshair and using a virtual crosshair afterwards, which stays in the same position in the image under ideal conditions. Since we estimate the heading using only the x -direction chessboard lines and we need no crosshair line directions, this would mean fixating one point in the image and using it as AMR position. In the experiments with our low-cost robot that has limited mechanical stability, we have found that using the laser diode, which is lightweight and mounted much closer to the ground than the camera, is more accurate and robust than using a virtual crosshair due to less vibrations and shaking of the laser diode.

D. Chessboard square detection

To detect the chessboard squares, we first apply a Canny filter for edge detection after grayscale conversion and Gaussian smoothing, as shown in Fig. 4b. The binary Canny output is then processed by Hough transformation to find

the chessboard lines. For further denoising, the detected lines are broadened and the image of lines is processed by an opening operation, which consists of erosion followed by dilation. In erosion and dilation, a 2D kernel is slid over the image, where the kernel center corresponds to the pixel to process. In each kernel, erosion only keeps white (detected line) pixels if all kernel pixels are white. Dilation does the opposite and sets the color of the center pixel to white if any pixel in the kernel is white. The image after Hough transformation and opening is depicted in Fig. 4c. For further operations, the image is inverted, as seen in Fig. 4d. The chessboard squares are detected by first finding and simplifying the white square contours with the functions `findContours` [30] and `approxPolyDP` [31], [32]. The simplified contours (polygons) are then filtered for square detection. Only polygons that have four edges, relative side lengths between factor 0.95 and 1.05, and an area of 80.000 - 100.000 pixels are kept. As the detected squares are slightly smaller due to the line broadening and opening, 10 pixels are added to the square corner coordinates. Those detected squares are given in Fig. 4e. In the last step, the detected corners are refined to subpixel accuracy with `cornerSubPix` [33] as shown in Fig. 4f.

If squares are occluded, the redundancy in the chessboard pattern enables estimating all squares (including the square with crosshair used for positioning) by simply extending the detected squares to build virtual, undetected squares. Given the precise square detection, this method has proven quite accurate. If for some reason no square is detected, we apply a constant velocity model for x , y and θ to estimate the AMR position and heading, which is sufficient for a high enough sampling frequency of camera images.

E. Position and heading estimation

Given the detected corner points of the chessboard square with detected laser crosshair, we compute the relative position of the crosshair in the square. We then convert the crosshair pixel coordinates to global coordinates with the known square size of $16.\bar{6}$ cm. To resolve the rotation ambiguity of the local square coordinate system and compute global world coordinates, the QR code references are used, as previously shown in Fig. 1b. The heading is computed as the angle between the chessboard lines in x -direction and the calibrated vertical image direction.

If no QR code is detected, we predict the current heading using a constant velocity model. The heading is then estimated by choosing the detected angle from the set of four ambiguous angles (due to the lack of knowledge which chessboard lines point in x - and y -direction) by a nearest neighbor assignment. The four ambiguous chessboard line directions are computed by clustering and averaging the lines from Hough transformation depicted in Fig. 4c. Since the AMR has to move in a physically plausible way and the heading cannot make large jumps between two images, this nearest neighbor assignment works reliably.

AMR position estimation is also possible without QR codes through crosshair tracking in a simple fashion. Since we

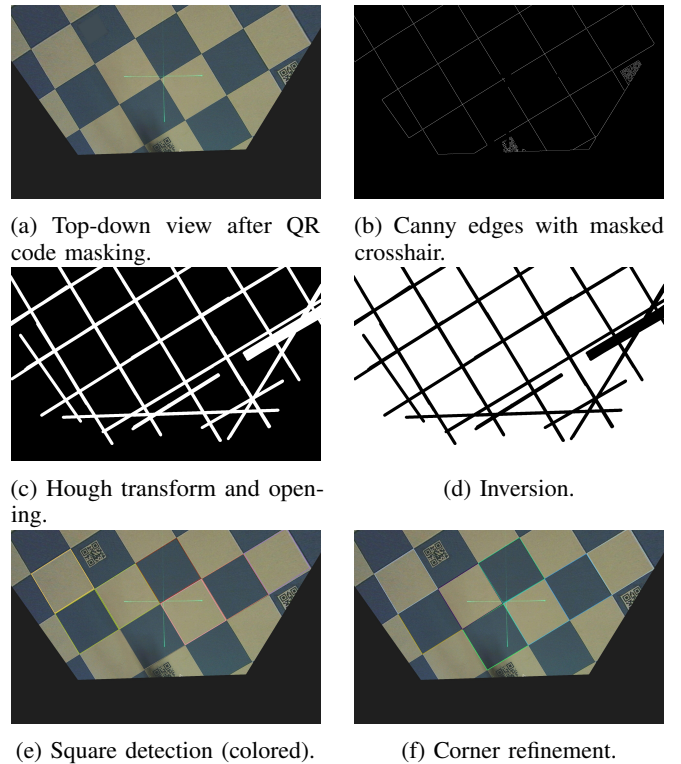


Fig. 4: Square detection process in the perspective transformed top-down image.

can reliably estimate the heading, no position ambiguity in local square coordinates occurs while tracking the crosshair, as the order of P1-P4 in Fig. 1b, i.e. the orientation of a locally observed square, stays known. To catch jumps between squares, we check if the crosshair position in local square image coordinates in x or y surpasses a threshold of 150 pixels and if so, we perform a global square jump in the respective direction.

Using this crosshair tracking after an initial global position and heading estimate with a QR code, further frequent global updates with the QR code references are not necessary, but this requires a high enough image sampling frequency such that the Nyquist-Shannon sampling theorem holds. The spatial frequency $f_{pattern}$ of the chessboard pattern is $f_{pattern} = \frac{1}{16.\bar{6}} \text{ cm}^{-1}$ and thus the images have to be sampled with a spatial frequency of at least $f_{image} = 2f_{pattern}$ to avoid aliasing (causing jumps into the wrong square while crosshair tracking). This upper bounds the maximum AMR velocity to $v_{max} = f_{image}^{-1} f_{fps}$, where f_{fps} is the sampling rate of the camera. We record with $f_{fps} = 8.\bar{3}$ Hz, i.e. $v_{max} \approx 0.69 \frac{\text{m}}{\text{s}}$, which is more than double of the maximum velocity of our AMR. To adapt the crosshair tracking for faster AMRs, one would have to either increase the unambiguous region (e.g. by increasing the square size), increase the sampling rate of the camera, or add a robust and accurate crosshair position prediction model (e.g. through odometry).

If no QR code is detected in the first frames, we assume an initial position and heading of $[x, y, \theta]^T = [0, 0, 0]^T$ and then

correct the initial estimates through rotation and translation once a QR code is available.

IV. EXPERIMENTS

A. Hardware

Our prototype AMR is a low-cost Raspberry Pi robot (SunFounder Picar-X) with Ackermann kinematics [34]. The USB RGB fisheye camera is from Sypro and offers a resolution of 1920x1200 pixels, a FoV of $> 150^\circ$, and fast image creation (i.e. negligible motion blur) by employing a global shutter. The green laser diode is from CTRICALVER with a wavelength of 520 nm and has less than 1 mW of power. The chessboard floor is made from Polyvinylchlorid (PVC) with a known square size of (16.6, 16.6) cm. Such floors can currently be bought for around 5-10 \$ per square meter in our region.

B. Localization experiments

To showcase the correct working of our system under real inference conditions with possible motion blur, vibrations etc., we drive the AMR in the laboratory by steering it wirelessly with a PS4 controller. Since hand-collecting ground truth on the floor [14] (e.g. with a set square and a protractor) is an error prone and tedious task that only works in a static setting, we developed a software tool to label the ground truth position and heading based on the corresponding top-down image by hand. We therefore zoom in and select the crosshair center and three points of the respective square to build the coordinate system for positioning, including the x -direction line for heading estimation. The points are selected to the best of our abilities with pixel accuracy, where one pixel equals roughly $\frac{16.66}{300} \simeq 0.56$ mm (see Fig. 1b).

V. RESULTS

The labeled and estimated trajectories are shown in Fig. 5. As visible, the estimates closely follow the ground truth.

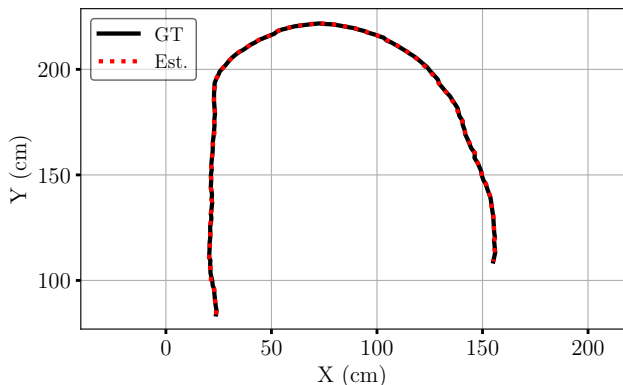
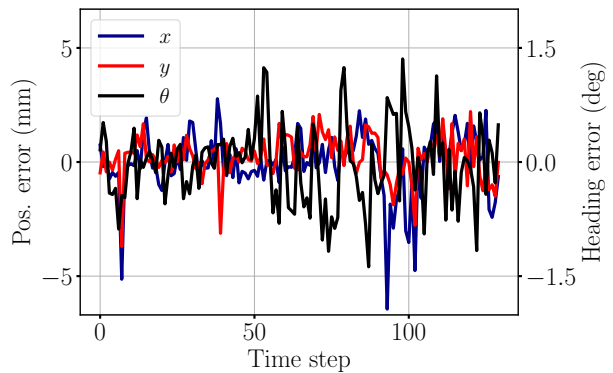
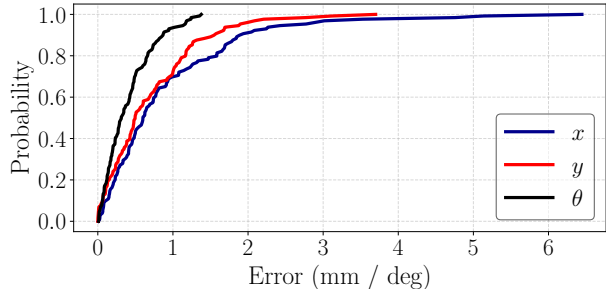


Fig. 5: Trajectory evaluation

A closer error evaluation is found in Fig. 6. The errors in x , y and θ are depicted in Fig. 6a. A few outliers arise due to small errors in the crosshair or corner detection, often caused by overlaps of the crosshair with the chessboard lines and corners. The corresponding CDFs of the absolute errors



(a) Errors.



(b) Cumulative density functions of the absolute errors.

Fig. 6: Position and heading errors in a) and corresponding CDFs of absolute errors in b).

are found in Fig. 6b. They show clearly that most errors in x and y are in low mm or even sub-mm range.

Table. I gives the bias, the mean absolute error (MAE), the maximum absolute error (Max), and the 95th and 99th percentiles of the absolute error for each parameter. All

TABLE I: Error statistics for x and y in mm and for θ in degrees.

	Bias	MAE	95th	99th	Max
x	-0.03	0.92	2.62	5.03	6.44
y	0.02	0.69	1.89	3.02	3.70
θ	-0.05	0.42	1.09	1.43	1.47

estimates have negligible bias. Positioning errors in both dimensions are similar as expected. The errors in x are higher due to more outliers as visible in Fig. 6a. The 99th percentile of the absolute errors and the max errors in x and y are well below 1 cm.

Heading estimation also shows good performance with the 95th percentile of absolute heading errors just slightly being over 1° and a non-negligible part of this error likely being due to the labeling process. Good heading accuracy is important to accurately map from the crosshair center to another position around the crosshair, e.g. to a localization sensor on the AMR.

VI. DISCUSSION

Our proposed GG system is low-cost and gives mm accuracy. It is, however, just a prototype and this localization approach brings several advantages and can be further improved upon.

Cost and portability: Our system is low-cost due to the low hardware requirements (camera, chessboard, processor, optional laser diode). We are confident that the system will also work with even cheaper hardware. The largest cost factor is currently the chessboard floor. However, any grid pattern is sufficient. For rooms without such chessboard floor, one might e.g. build a grid by projection orthogonal laser lines on the floor using a laser level and drawing or taping such line pattern on the floor using the laser lines. One may also build a portable version, where pre-built chessboard grid patches can be stucked together. The system can further work with a cheaper camera and since the image processing is relatively simple, one might implement a future (online) version that runs on a field programmable gate array (FPGA).

Accuracy: Due to the high spatial resolution of modern cameras and the closeness of the camera to the position references (chessboard corners) and the crosshair on the ground, we achieve high positioning accuracy. The localization accuracy of GG is also mostly independent of the AMR position in the room, given similar illumination conditions. Performance might be enhanced by multi-camera and multi-laser setups. The localization method could be extended to handle arbitrary detected chessboard corners, opposed to the four square corners in which the crosshair lies. Our current positioning bottleneck (with a moving AMR) is the not the localization algorithm, but the mechanical stability of the AMR, which causes larger shaking and vibration of the camera, and to a smaller extend also of the laser diode and the crosshair. The resulting position and heading jitter is not considered in our evaluation. Simple hardware improvements include an AMR with better stability, more rigid camera and laser diode installations, and stabilizers for the camera and also for the laser diode in case of localization using a real crosshair. On the software side, smoothing the trajectory, e.g. online with an alpha-beta or a Kalman filter [35], or offline with a Savitzky-Golay [36] filter, would reduce this jitter.

3D position and orientation estimation: An alternative localization approach that could be studied in future work is Perspective-n-Point (PnP)-based localization with a monocular camera, as often used with fiducial markers and realized in a conceptionally similar system to ours with a hand-held camera and a small, printed chessboard in [37]. Therefore, the known correspondences between the detected 2D chessboard corner points in the image and their known 3D positions in world coordinates enable 3D camera position and orientation estimation without the laser diode. While potentially less accurate in 2D position estimation, this could minimize the error from projecting the estimated position by GG to the position of another localization sensor on the AMR. The current localization method could theoretically employ a (virtual) crosshair located on the floor below the AMR for

positioning. However, this requires installing the camera and additional lighting at the bottom of the AMR chassis and dealing with very small camera-ground distance (motion blur & visibility of full chessboard squares).

Global localization: By equipping the floor with QR codes, we achieve absolute, global localization capabilities. QR codes were, however, just a readily available solution for this proof-of-concept of the system. Simpler visual encodings that are easier and faster to detect would improve the system, especially for an online version. The encodings are used to identify the chessboard square corners, e.g. with the known QR corners as in our current version, or by other means such as making the different grid lines identifiable.

Real-time processing: In addition to the implemented crosshair tracking and the proposed FPGA version, simpler global position and orientation references etc., the image processing still has much potential for improvement. Instead of running the full QR code, crosshair and corner detection for each image as described in Sec. III (which itself has room for improvement, e.g. by applying a simpler method run at lower resolution to find the initial chessboard corners instead of the expensive Hough transformation at full resolution), one might track the global references and the periodic chessboard corners after initial detection and make use of the prior knowledge about the crosshair position in the image. This would require processing only smaller patches of the images, thus speeding up the detection chain.

Robustness: The redundant, periodic chessboard pattern allows our system to work even if large areas of the chessboard are occluded, e.g. by other AMRs, people, dirt etc. Since the crosshair stays roughly in the same position of the image and parts of the crosshair are sufficient for crosshair detection, we can also deal with crosshair occlusion. Robustness could be further increased by adding more cameras, laser diodes, and odometry, which would additionally improve accuracy, but also increase system complexity and cost. Moreover, the crosshair could be replaced by a more redundant laser pattern.

Scalability: Our GG system is scalable to large areas. In addition, the system can be scaled to robot swarms. In a version without the laser diode (virtual crosshair or PnP), there will be no interference between robots except for some floor occlusion, which the system can handle. If all robots use the same laser diode, one can still differentiate the different laser crosshairs, as the crosshair of each respective robot stays in the same place in the images. In case there might be interference between the crosshairs, one could try installing lasers of different colors or patterns on the robots.

VII. CONCLUSION

We have introduced a novel, camera-based indoor localization system called GroundGazer (GG) for 2D AMR position and heading estimation. Opposed to currently existing methods with similar mm localization and sub-degree heading accuracy, our system has much lower hardware requirements. Its limitation is the need for a chessboard or a similar grid pattern and global position and orientation references on the floor, which may limit its usability for applications where this

is impractical. We built a prototype of GG using a chessboard floor with known corner coordinates as passive position references, QR codes as global position and orientation references, a ground gazing fisheye camera placed at low height on the AMR, and a laser diode that projects a crosshair from the AMR onto the chessboard floor. The crosshair on the floor is continuously observed by the camera for position and heading estimation. Our prototype achieved low mm localization and sub-degree heading accuracy. We have further discussed the many advantages this localization approach brings and how it may be improved and extended in various directions in future work.

REFERENCES

- [1] R. Mautz, *Indoor positioning technologies*. Habilitation thesis, ETH Zürich, Zürich, 2012.
- [2] A. Yassin, Y. Nasser, M. Awad, A. Al-Dubai, R. Liu, C. Yuen, R. Raulefs, and E. Aboutanios, "Recent advances in indoor localization: A survey on theoretical approaches and applications," *IEEE Communications Surveys & Tutorials*, vol. 19, no. 2, pp. 1327–1346, 2017.
- [3] R. Mautz and S. Tilch, "Survey of optical indoor positioning systems," in *2011 International Conference on Indoor Positioning and Indoor Navigation*, pp. 1–7, 2011.
- [4] A. Morar, A. Moldoveanu, I. Mocanu, F. Moldoveanu, I. E. Radoi, V. Asavei, A. Gradinaru, and A. Butean, "A comprehensive survey of indoor localization methods based on computer vision," *Sensors*, vol. 20, no. 9, 2020.
- [5] F. Euchner and S. ten Brink, "Espargos: Phase-coherent WiFi CSI datasets for wireless sensing research," in *2024 Kleinheubach Conference*, pp. 1–4, 2024.
- [6] K. M. Bae, H. Moon, S.-M. Sohn, and S. M. Kim, "Hawkeye: Hectometer-range subcentimeter localization for large-scale mmwave backscatter," in *Proceedings of the 21st Annual International Conference on Mobile Systems, Applications and Services, MobiSys '23*, (New York, NY, USA), p. 303–316, Association for Computing Machinery, 2023.
- [7] M. Vossiek, R. Roskosch, and P. Heide, "Precise 3-D object position tracking using FMCW radar," in *1999 29th European Microwave Conference*, vol. 1, pp. 234–237, 1999.
- [8] ZeroKey, *Quantum RTLS™ 2.0 Datasheet*, Oct. 2024. Accessed: August 31, 2025. Available: <https://zerokey.com/wp-content/uploads/2024/10/Quantum-RTLS-2.0-Datasheet.pdf>.
- [9] J. Ma, F. Zhang, B. Jin, S. Li, and Z. Wang, "MULoc: Towards millimeter-accurate localization for unlimited UWB tags via anchor overhearing," in *IEEE INFOCOM 2025 - IEEE Conference on Computer Communications*, pp. 1–10, 2025.
- [10] J. Ma, L. Qiao, Z. Wang, S. Dang, and M. Beach, "Millimeter accuracy indoor localization system using an attention convolution model," in *2024 IEEE Wireless Communications and Networking Conference (WCNC)*, pp. 1–5, 2024.
- [11] Z. Gong, S. Yu, B. Tao, Z. Gu, J. Wang, and H. Ding, "The visual fiducial based pose estimation of mobile manipulator in large-scale components manufacturing," *Science China Technological Sciences*, vol. 64, p. 2186–2199, July 2021.
- [12] G. Bolanakis, K. Nanos, and E. Papadopoulos, "A QR code-based high-precision docking system for mobile robots exhibiting submillimeter accuracy," in *2021 IEEE/ASME International Conference on Advanced Intelligent Mechatronics (AIM)*, pp. 830–835, 2021.
- [13] R. Mautz, "The challenges of indoor environments and specification on some alternative positioning systems," in *2009 6th Workshop on Positioning, Navigation and Communication*, pp. 29–36, 2009.
- [14] D. Becker, F. Thiele, O. Sawade, and I. Radusch, "Cost-effective camera based ground truth for indoor localization," in *2015 IEEE International Conference on Advanced Intelligent Mechatronics (AIM)*, pp. 885–890, 2015.
- [15] S. Thrun, W. Burgard, and D. Fox, *Probabilistic robotics*. Cambridge, Mass.: MIT Press, 2005.
- [16] K. Kozak and M. Alban, "Ranger: A ground-facing camera-based localization system for ground vehicles," in *2016 IEEE/ION Position, Location and Navigation Symposium (PLANS)*, pp. 170–178, 2016.
- [17] L. Zhang, A. Finkelstein, and S. Rusinkiewicz, "High-precision localization using ground texture," in *2019 International Conference on Robotics and Automation (ICRA)*, pp. 6381–6387, 2019.
- [18] X. Chen, A. S. Vempati, and P. Beardsley, "Streetmap - mapping and localization on ground planes using a downward facing camera," in *2018 IEEE/RSJ International Conference on Intelligent Robots and Systems (IROS)*, pp. 1672–1679, 2018.
- [19] J. Fabian Schmid, S. F. Simon, and R. Mester, "Ground texture based localization using compact binary descriptors," in *2020 IEEE International Conference on Robotics and Automation (ICRA)*, pp. 1315–1321, 2020.
- [20] P. Brömmel, D. Brämer, O. Urbann, and D. Kleingarn, "Robot localization using a learned keypoint detector and descriptor with a floor camera and a feature rich industrial floor," *arXiv preprint arXiv:2504.03249*, 2025.
- [21] C. Patrino, R. Colella, M. Nitti, V. Renò, N. Mosca, and E. Stella, "A vision-based odometer for localization of omnidirectional indoor robots," *Sensors*, vol. 20, no. 3, 2020.
- [22] J. Zheng, S. Bi, B. Cao, and D. Yang, "Visual localization of inspection robot using extended Kalman filter and Aruco markers," in *2018 IEEE International Conference on Robotics and Biomimetics (ROBIO)*, pp. 742–747, 2018.
- [23] Z. Liu, W. Qin, Z. Li, and G. Zhou, "Multi-tag fusion localization method based on geometric constraints," *Applied Sciences*, vol. 14, no. 13, 2024.
- [24] P. Nazemzadeh, D. Fontanelli, D. Macii, and L. Palopoli, "Indoor localization of mobile robots through QR code detection and dead reckoning data fusion," *IEEE/ASME Transactions on Mechatronics*, vol. 22, no. 6, pp. 2588–2599, 2017.
- [25] T.-W. Kang and J.-W. Jung, "A drone's 3D localization and load mapping based on QR codes for load management," *Drones*, vol. 8, no. 4, 2024.
- [26] G. C. L. Delfa, S. Monteleone, V. Catania, J. F. D. Paz, and J. Bajo, "Performance analysis of visual markers for indoor navigation systems," *Frontiers of Information Technology & Electronic Engineering*, vol. 17, no. 8, pp. 730–740, 2016.
- [27] S. Hinderer, M. Scheffler, and B. Yang, "Investigation of ArUco marker placement for planar indoor localization," in *2025 IEEE International Conference on Advanced Robotics (ICAR)*, pp. 606–613, 2025.
- [28] G. Bradski, "The OpenCV Library," *Dr. Dobbs's Journal of Software Tools*, 2000.
- [29] R. O. Duda and P. E. Hart, "Use of the Hough transformation to detect lines and curves in pictures," *Commun. ACM*, vol. 15, p. 11–15, Jan. 1972.
- [30] S. Suzuki and K. be, "Topological structural analysis of digitized binary images by border following," *Computer Vision, Graphics, and Image Processing*, vol. 30, no. 1, pp. 32–46, 1985.
- [31] U. Ramer, "An iterative procedure for the polygonal approximation of plane curves," *Computer Graphics and Image Processing*, vol. 1, no. 3, pp. 244–256, 1972.
- [32] D. H. Douglas and T. K. Peucker, "Algorithms for the reduction of the number of points required to represent a digitized line or its caricature," *Cartographica*, vol. 10, no. 2, pp. 112–122, 1973.
- [33] W. Förstner and E. Gülch, "A fast operator for detection and precise location of distinct points, corners and centres of circular features," in *Proceedings of the ISPRS Intercommission Conference on Fast Processing of Phonogrammic Data*, pp. 281–305, 1987.
- [34] K. M. Lynch and F. C. Park, *Modern Robotics: Mechanics, Planning, and Control*. USA: Cambridge University Press, 1st ed., 2017.
- [35] Y. Bar-Shalom, X. Li, and T. Kirubarajan, *Estimation with Applications to Tracking and Navigation: Theory, Algorithms and Software*. John Wiley & Sons, Inc., 2002.
- [36] A. Savitzky and M. J. E. Golay, "Smoothing and differentiation of data by simplified least squares procedures.," *Analytical Chemistry*, vol. 36, no. 8, pp. 1627–1639, 1964.
- [37] M. Solony, P. Zak, V. Beran, and M. Spánel, "Camera localization using incomplete chessboard pattern," in *Proceedings of the International Conference on Computer Vision Theory and Applications - Volume 1: VISAPP, (VISIGRAPP 2011)*, pp. 415–418, INSTICC, SciTePress, 2011.